Citrate Effect on the Swelling Behaviour and Stability of Casein Microparticles

Md Asaduzzaman
RWTH Aachen University
Thomas Pütz
RWTH Aachen University
Ronald Gebhardt (ronald.gebhardt@avt.rwth-aachen.de)
RWTH Aachen University

Research Article

Keywords: casein microparticles, swelling, citrate, dynamic modeling

Posted Date: April 18th, 2022

DOI: https://doi.org/10.21203/rs.3.rs-1554501/v1

Version of Record: A version of this preprint was published at Scientific Reports on November 1st, 2022.
See the published version at https://doi.org/10.1038/s41598-022-23096-x.

Abstract

Casein microparticles obtained from casein micelles by volume exclusion of added pectin and subsequent film drying remain stable in the acidic and neutral pH range, but swell strongly in the basic range. Calcium significantly determines the stability and water-binding behavior of phosphorylated caseins and the aggregates and gels formed from them. For a future effective and controlled use as a carrier for bioactive substances, e.g. via the gastrointestinal tract, we therefore investigated how the addition of the calcium chelating agent citrate affects the swelling and stability of the microparticles. Concentrations of 2 mM and more citrate cause a stronger swelling of the microparticles at pH 8 and by means of 4 mM and more the second characteristic swelling step can also be investigated within the observation time of 120 minutes, since it starts earlier. All swelling kinetics can be simulated using seven parameters of a dynamic model, which reproduces the individual swelling steps via volume inflows and outflows into a reservoir. While the rate coefficient for swelling step 1 increases linearly with the citrate concentration, no such dependence could be found for swelling step 2. The more citrate is used, the faster the microparticles decompose in turbidity experiments after the addition of sodium dodecyl sulfate, which can be related to a weakening of the hydrophobic interactions.

Introduction

Demand for biopolymer-based microparticles is continuously increasing. Microparticles are used, for example, as colloidal delivery systems in food, drug and biomedical applications to encapsulate, protect and release bioactive ingredients. Protein-based biopolymers offer promising advantages over synthetically produced materials such as their biocompatibility, biodegradability, low immunogenicity, antibacterial activity, lower risk of side effects, and low cost (Zahrriev et al 2021, DeFrates et al, 2018). As natural carriers of bioactives, milk proteins possess many structural and physicochemical properties to functionalize them for transport and delivery tasks (Livney 2010). Caseins are a particularly promising material for microparticulate delivery systems because they occur unfolded in the native state, have a high water- and calcium-binding capacity as well as a strong tendency to self-assemble into higher aggregated structures and exhibit a high affinity for binding hydrophobic substances due to their amphiphilic nature (Sadiq et al. 2021, Zahrriev et al. 2021).

In bovine milk, four types of casein (α_{S1}-, α_{S2}-, β- and κ-casein) form together with calcium phosphates spherical association colloids with average sizes between 100 to 300 nm (Dalgleish and Corredig 2012). Caseins can be simplified as block copolymers to explain their adsorption behavior and assembly (Horne 2002). In this modeling approach, the caseins consist of alternating clusters of phosphoseryl-residues interacting with colloidal calcium phosphate and hydrophobic blocks through which caseins are interconnected. Colloidal stability is provided by κ-casein, which forms an extended polymer brush on the micellar surface (de Kruif and Zhulina 1996). Casein micelles are highly hydrated with about 3.3 g water per g of protein, with a portion directly bound to the protein and others associated with the κ-casein polymer brush on the surface but the main portion with 1.8 g/g is entrapped in voids or water-filled channels in the micellar structure (Huppertz et al. 2017). A sponge-like internal structure with water-rich

and water-poor regions was proposed as a model for casein micelles (Dalgleish 2011) based on experimental studies (Bouchoux et al 2010, McMahon and Oommen 2008). Besides phosphate and chloride, citrate is a major anion in the aqueous phase of milk and acts like polyphosphates and EDTA as a calcium chelator (Broyard and Gaucheron 2015). Indeed, added citrate demineralizes casein micelles by indirectly dissolving colloidal calcium phosphate (Huppertz et al., 2007; Huppertz and deKruif, 2008). As the interactions between phosphoseryl residues and calcium are reduced, the caseins become negatively charged, so that their water-binding capacity is increased. Studies with high hydrostatic pressure (Gebhardt et al. 2011) or by using denaturants such as sodium dodecyl sulfate (SDS) (Lefebvre-Cases et al 1998, Liu and Guo, 2007) have demonstrated the importance of hydrophobic interactions for the internal structural stability of casein micelles.

The typical process of producing microparticles involves gel formation, emulsification, spray drying, heat treatment, etc. (Zhuang et al., 2016, Marreto et al., 2013, Yang et al., 2020). Instead, we applied a gentle method of microparticles production based on depletion flocculation reaction in a casein-pectin system at pH 6.8 (Zhuang et al., 2015). Under this process, the casein-pectin attractive interaction is not dominant but the voluble exclusion by pectin is responsible for the formation of casein aggregates (de kruif and Tuiner 2001). Stable microparticles were formed by film drying followed by enzymatic hydrolysis of the pectin film matrix. The produced CMP was then suspended in buffer solution at pH 6.8. The resulting CMPs have been reported to have a spherical shape and are stable in BisTris buffer at 4°C for 21 days (Schulte et al 2020b). Usually, other casein-rich hydrogel systems tend to degrade or swell at acidic pH (Chang et al. 2017). However, CMPs prepared by depletion flocculation reaction exhibit remarkable stability under an acidic environment. For instance, at pH 14 it took only a few seconds, at pH 8 a few hours, and at pH 0 no practical swelling are observed (Schulte et al. 2020a). As the pH in the human stomach is highly acidic and near neutral in the duodenum (Hens and Bolver 2018), the pH-dependent stability and swelling properties of CMPs can be favorable for the controlled release of the orally supplemented bioactive compounds. Being amphiphilic caseins have the affinity to bind both hydrophobic bioactive compounds such as vitamins, and/or hydrophilic compounds such as polysaccharides. Moreover, the unfolded structure of casein allows them more accessible to proteolytic enzymes in the gastrointestinal tract resulting in better release properties (Sadiq et al 2021, Livney 2010).

It is important to know the characteristic properties and stability of the produced microparticles before functionalization to protect and use the encapsulated material effectively. The microparticle produced under depletion flocculation have a highly porous inner structure that expands during swelling (Schulte et al 2021). The concentration of $CaCl_2$ in the running solution has a significant effect on the swelling behavior of the microparticles as well. For instance, adding 0.1 mM $CaCl_2$ at pH 11 slowed the two-phase linear growth of the particle area. In contrast, at a concentration of > 10 mM $CaCl_2$ almost no swelling of the CMP was observed (Schulte et al., 2020b). Free calcium and calcium phosphate nanoclusters facilitate cross-links between the negatively charged casein chains. Such neutralization of charges further enables hydrophobic contracts between caseins and strengthening of the inner structure particle (De Kruif et al., 2012). The results of stability experiments indicate that hydrophobic interactions are

essential for maintaining the overall structure, as CMPs decompose completely upon addition of sodium dodecyl sulfate (SDS) (Schulte et al. 2021).

The application of casein microparticles for a sustainable delivery system of bioactive compounds is of great interest. Due to the characteristic pH-dependent swelling behavior, CMPs could be used in the future for microencapsulation through gastric passage and controlled intestinal release of bioactive compounds. With the dosed use of Ca-chelatants during production, the charge state and the water-binding behavior of CMPs could be changed and thus their swelling behavior be adjusted in a controlled manner. Therefore, in this study, the effect of citrate on the stability and swelling behavior of CMPs at two relevant pH values is investigated.

Material And Methods

Materials

Casein micelle concentrate (CMC) powder MC 80 was kindly provided by Milei GmbH Germany and citrus pectin (classic CU 201) was from Herbstreith & Fox (Herbstreith & Fox GmbH & Co. KG, Neuenbürg, Germany). Pectinase from *Aspergillus niger*, Tri-Sodium citrate, hydrochloric acid (1M), Sodium hydroxide (1M), and Sodium azide was from Merck (Merk, Darmstadt, Germany). Especially pure sodium dodecyl sulfate (SDS), ultra-pure BisTris, calcium chloride, and all salts (purity >99% or analytical grade) for SMUF preparation were obtained from VWR, Radnor, USA. Milli-Q water was obtained from our lab.

Preparation of working solutions

BisTris buffer solution (50 mM BisTris, 10 mM $CaCl_2$) was prepared by adding 10.462 g BisTris in a volumetric flask containing about 980 ml milli-Q water under continuous stirring. After complete dissolution, 1.11 g $CaCl_2$ was added to the solution and allowed to dissolve completely. The pH of the solution was adjusted to 6.8 with 1M HCl and NaOH and finally filled the volume up to 1L.

Simulated milk ultra-filtrate (SMUF) solution was prepared according to a protocol described by Dumpler et al 2017. All salts were dissolved step by step, allowing the complete dissolution of the previous salt then the next salt was added. Finally, pH was adjusted at 6.8 with 1M HCl and NaOH.

Pectin solution (2%) was prepared by dissolving 1 g Pectin in 49 g BisTris buffer solution with vigorous stirring at 80°C for 3 h then cooled down to room temperature. Finally, pH was adjusted to 6.8 with 1M HCl and NaOH.

Casein dispersion (7.36%) was prepared by dissolving 2 g of the CMC powder (protein >80% of which >92% casein) in 18 g of SMUF. The CMC powder was allowed to dissolve under continuous stirring at room temperature for 1 followed by 4 h at 4°C and finally 1 h at 37°C. To avoid microbial contamination, 0.5 $g.L^{-1}$ sodium azide was added to the dispersion. For the preparation of citrate-treated CMP, the

required amount of Tri-sodium citrate solution (200 mM in water) was added during the final 1 h stirring steps of casein dispersion.

Pectinase solution (activity ≈ 36 units/ml) was prepared by adding 0.47 ml pectinase (activity ≈ 800 units per ml) from *Aspergillus niger* to 10 g BisTris buffer and mixed properly. The solution was prepared immediately before adding to the film.

Preparation of Casein microparticle (CMPs)

The principle of the CMP production process was based on the depletion flocculation interaction between casein micelles (CMs) and pectin (Tuinier et al. 1999). The individual preparation steps are summarized in Fig. 1. The preparation of the CMPs was according to a protocol described by Schulte et al 2021. Briefly, the casein solution, pectin solution, and BisTris buffer solution mentioned above were mixed properly in a proportion of 4.1:1.5:4.4 (w/w) to obtain 3.0% casein and 0.3% pectin in the final solution. Then 3.9 g of this mixed solution was transferred to a glass petri dish (Ø 70 mm) and dried at room temperature for 16 h to produce a film. To hydrolyze this film 10 g pectinase solution was added to the petri dish. The enzymatic hydrolysis was performed in a ThermoMixture (Eppendorf, Eppendorf AG, Hamburg, Germany) at 47°C for 2 h with 160 rpm. After hydrolysis, the supernatant solution was collected in a falcon tube and centrifuged at 22°C and 1500 RFC for 10 min. The clear solution was poured out from the top and the resulting stabilized pellet of CMPs was then suspended again in BisTris buffer and stored at 4°C for further use.

Swelling experiments

The swelling behavior of CMP was studied according to the protocol developed by Schulte et al 2020a. Briefly, the swelling chamber was filled with CMP dispersion (in BisTris buffer, pH 6.8) and placed under Leica DMIL LED inverted microscope (Leica Microsystems, GmbH, Wetzlar, Germany) connected with Basler camera (Basler AG, Ahrensburg, Germany). The dispersion was allowed to stand for approx. 10 min to sediment the CMP into the sieve holes. A PHD ULTRA™ syringe pump (Harvard Apparatus, MA, USA) was connected with the swelling chamber by polyethylene tubes (Ø 0.55 mm). The pump flow rate was set at 0.05 ml per min for the exchange medium (ultrapure water, pH, 3 or 8). The swelling process of the CMP at different pH was started by replacing the buffer solution with an exchange medium. With the activation of the syringe pump, an image of a single CMP trapped in the sieve holes was started to record (at the rate of 2 frames per second for 2 h) using the Basler video recording software. Image frames were extracted using PyCharm (version 2021.1.3, JetBrains, Czech) and the area of the CMPs was calculated by a freehand selection of particles outer lines using ImageJ software (NIH, USA). All samples were measured in duplicate.

Dynamic swelling model and data analysis

For a more detailed analysis of the swelling behavior, the cross sections of the CMPs in the micrographs were first evaluated and plotted as a function of swelling time. The influence of citrate on the typical two-

stage swelling behavior of the CMPs can be simulated with a dynamic model whose basic structure has already been described (Schulte et al., 2020b). Volumes are first calculated from the determined cross-sectional areas for the simulation, assuming the spherical approximation that is satisfied for the swelling process (Schulte et al., 2021). Within the model, the volume changes by two inflows and two outflows, respectively, which are controlled by valves. All incoming and outgoing volume flows are proportional to the current volume of the CMPs at each time point. The rate coefficients for the inflows and outflows assume a time-invariant value after a characteristic time through a step function (or through a transition function as exemplified in Fig. 3). The model is able to describe all measured swelling kinetics in a good approximation by a maximum of 9 parameters (4 characteristic times and 4 rate coefficients as well as an initial value for volume or particle area). The numerical integration of the underlying differential equations was performed with the program Stella, isee systems.

Stability experiments

For stability analysis, turbidity of CMPs solution was monitored using a Lambda 365 UV/VIS spectrometer (PerkinElmer, USA) according to the method described by Schulte et al 2021 with slight modification. Briefly, 1.5 ml CMP dispersion was filled in semi-micro cuvette (Eppendorf AG, Germany) and BisTirs buffer was used as reference. The turbidity was measured at a wavelength of 600 nm, slit width of 1 nm and absorbance was recorded for 900 s. Immediately after measurement, 40 µl SDS solution (520 mM in water) was added to CMP dispersion resulting in a 13.5 mM final concentration of SDS. The cuvette was then gently up and down 3 times to properly mix the SDS, placed back in the spectrometer, and measured again. All samples were measured in duplicate.

Results And Discussion

We prepared CMP at different citrate concentrations and performed swelling and stability experiments with the resulting particles at pH 8 and pH 3. The microscpic images in Fig. 2 show the circular cross sections of the particles in the used swelling cell at the beginning and 120 min after the pH change to pH 8 and to pH 3, respectively. While there is a significant increase in cross-sectional area at pH 8, no change can apparently be seen at pH 3. Citrate is known to indirectly demineralize casein micelles by chelating ionic calcium in the aqueous phase (Broyard and Gaucheron 2015). As a result of the residual negative charge on the casein and the osmotic contribution of an increased content of counterions, the casein micelles become more hydrated and swollen (de Kort et al 2011, Huppertz et al 2007). This results in the increased swelling at pH 8 but not at pH 3. Under these conditions, caseins can be assumed to be in a stable gel state. CMs form an acid-induced gel below a pH of 5.2 because the stabilizing κ-casein brush border collapses (Tuinier and de Kruif, 2002). In addition, below the isoelectric point of casein (at pH 4.8), many amino acid residues of casein are are present in a protonated state, forming strong hydrogen bonds and further compacting the structure and preventing it from swelling (Liu and Guo, 2008). For detailed analysis, the cross-sectional areas of the CMPs from the image sequences of each of two individual swells were evaluated and averaged and plotted in the swell curves below.

The particle areas were related to those at the beginning of the swelling process where no exchange buffer was present in the swelling cell. A clear citrate effect on the degree of swelling and the course of the overall process can be seen based on the swelling kinetics. While the CMPs without citrate do not even double in particle size after 7200 s, maximum degree of swelling was achieved within this observation window for preparations with 8 mM citrate. For the CMPs prepared with less citrate, the degree of swelling at the end of the kinetics increases almost linearly with the citrate concentration. For CMPs without citrate influence, we have reported a two-step swelling process that finally resulted in the complete dissolution of the particles (Schulte et al., 2020a). We found that the particle area increased almost linearly with swelling time during both swelling steps, but first at a lower and then at a higher rate. While both steps of the overall process could be resolved well in the range of pH 11 to pH 14, this has only been possible to a limited extent at pH 8 due to the time-consuming swelling process under these relevant milieu conditions. In detail, only few swelling data could be collected for swelling step 2 until now at swelling times > 7000 s. However, with citrate treatment, the second swelling step of the CMPs can now be resolved. For the swelling curves at 4, 6 and 8 mM citrate, it starts after about 6000 s with nearly the same rate in each case. The rate of the first swelling step, however, increases more and more with citrate concentration. In contrast to the experiments without citrate addition, swelling step 2 does not occur immediately following swelling step 1. Instead, we observe an intermediate time period where the particle area increases less. This occurs, for example, in the swelling curve for 8 mM citrate at times between 2000 and 6000 s. We observed a similar phase of reduced swelling in the kinetics at pH 11 when 0.1 mM calcium and more was added to the exchange buffer (Schulte et al., 2020b). In this case, the addition of calcium results in further physical linkages that slow down and limit the swelling process.

For a more detailed analysis, we simulated the swelling kinetics with a dynamic model, which describes the different phases of particle swelling via different volume flows with respect to a reservoir. The phases of reduced expansion following the swelling steps, which were observed after the addition of calcium or in this case under the influence of citrate, can be simulated by additional volume flows out of the reservoir. The structure of the dynamic model used is described in detail in section 2.3. Figure 3 shows one of the swelling kinetics of CMPs for each of the citrate concentrations and for the reference without citrate addition along with the model simulations. In total, up to seven parameters were adjusted for the simulation of the kinetics.

The swelling kinetics of the CMP without citrate influence could be simulated using only one swelling step with a constant rate coefficient and a corresponding characteristic starting time. Under these conditions, there is no evidence of flattening of the swelling of the first step nor of the existence of a second swelling step, which may be due to both the comparatively large scatter of the data and the limited observation period of 7200 s. In contrast, CMPs prepared with 2 mM citrate swell faster but also exhibit a significantly longer lag phase before the swelling step begins. However, there is an abrupt change in the increase in particle area during swelling. After about 3000 s, the particles swell significantly slower with reduced but constant rate. The corresponding feature in the swelling curve can be simulated by a volume outflow with a characteristic rate coefficient over another step function with a time offset (see dotted line for the corresponding rate coefficient).

In the swelling kinetics of the CMP prepared with citrate concentrations of 4–8 mM, a second swelling step can be seen in addition to the first swelling step and subsequent region of reduced expansion. To simulate these swelling data, a volume inflow and outflow for swelling step 1 and a volume inflow for swelling step 2 were used with the corresponding rate coefficients for the time ranges plotted in the lower part of the graphs. Due to the jump functions used for the rate coefficients, discontinuities such as kinks occur in the simulations. Such a kink appears, for example, for the swelling of CMPs prepared with 8 mM citrate during the first swelling step at the transition to the decelerated phase (see dotted ellipse). The corresponding area of the swelling curve is magnified in the plot at the bottom right of Fig. 3. The simulation of the measured data can be significantly improved by adding another model parameter for the use of a transition function instead of a step function for the rate coefficient. Due to the internal structuring of the CMPs, it can be assumed that the physicochemical properties of a large number of structural elements determine the swelling process. In particular for the first swelling step, we assume that this is based on the expansion of a few µm-sized building-blocks within the CMPs. Since their composition and size are not uniform but distributed, it can be assumed that a changed swelling behavior follows a finite transition rather than a sharp step function.

The rate coefficients used for the simulation of the individual swelling steps are plotted over their corresponding characteristic times for all measured kinetics in Fig. 4. For comparison, the ranges of values obtained for the pH-dependent swelling of CMPs prepared without citrate are shown in an inset. For these reference samples, the swelling curves consisted of only two directly consecutive swelling steps. The double logarithmic plot shows that particularly high swelling rates and short times to the onset of each swelling step occur at pH 14, while the reverse is true at pH 8. All kinetic data at pH 8 collected in this study lie in the white-marked region and are thus clustered around the previously collected data without citrate at pH 8 (Schulte et al., 2022). The aim of using citrates was both to increase the swelling rates and to shorten the characteristic times until the onset of the swelling processes. Transferred to the insert in Fig. 4, this means a diagonal shift of the value ranges from the lower right at pH 8 to the upper left in the direction of pH 11. As can be seen from Fig. 4, under citrate influence, the rate coefficients for the first swelling step actually shift to higher values. In fact, we observe a linear increase of this rate coefficient as a function of citrate concentration as Fig. 5a shows. In contrast, there appears to be no citrate dependence for the rate coefficient of the second swelling step, as the values fluctuate around a constant value. The characteristic times, on the other hand, shift to higher values within the newly acquired data for the first swelling step, while no statements can be made for the second swelling step.

Thus, contrary to the assumptions, the time until the start of the first swelling step is not shortened by the citrate influence, but delayed by a few minutes. Furthermore, similar to the pH effect, citrate influences the rate coefficients for both swelling steps relative to each other. This can be seen by comparison with the reference samples analyzed at different pH values but without citrate influence in the insert in Fig. 4. While at pH 14 the rates of the second swelling step (open areas) are clearly larger than those of the first swelling step (black areas), this difference is less pronounced at pH 11. At pH 8, the areas of values for the rate coefficients of both steps are at the same level. After the addition of citrate, this trend is now continued, although the proton concentration is kept constant at pH 8. For all CMPs with citrate influence,

the rates of the second swelling step are lower compared to the first step. The reason for this is the positive citrate dependence of the first swelling step, which does not exist for swelling step 2 as shown in Fig. 5a. In addition to stronger swelling, we also observe increasing instability of the CMPs with increasing citrate concentration. This is indicated by turbidity experiments that resulted in monoexponential decay for all particle preparations after SDS addition as exemplified as an inset in Fig. 5b. The decay rates obtained after fit with an exponential function indicate more unstable CMPs by citrate. The destabilization can be attributed to a weakening of the hydrophobic interactions between the caseins (Lefebvre-Cases et al 1998, Liu and Guo, 2007). Since citrate primarily removes calcium from the caseins, which leads to a negative charge of the caseins, the weakening is probably a secondary effect caused by the increasing electrostatic repulsion.

Conclusions

CMPs show a strongly reduced swelling behavior at the physiologically important milieu condition of pH 8. On average, the swelling process must be observed under the microscope for two hours until the particle areas of the CMPs double. The aim of this study was to improve the swelling behavior by destabilizing the starting material, i.e. the CMs, by citrate during the manufacturing process of the CMPs. Our studies show a clear citrate effect on the swelling behavior and stability of the CMPs. When 8 mM citrate is used during preparation, we observe that the particle areas of the resulting CMPs swell to more than four times their initial size at pH 8. Moreover, our results show that the more citrate was used, the faster the first step of the two-step swelling process occurs. In addition to the occurrence of a phase with reduced swelling velocity within the first swelling step, we further observe that under the influence of citrate the entire swelling process accelerates to such an extent that the second swelling step can also be investigated. The improved swelling behavior at pH 8 and the lower stability of CMPs prepared with citrate might favor the release of the encapsulated substances under basic conditions such as in the intestine and should be investigated in further studies.

Declarations

Acknowledgements

We thank Jann Schulte for helpful discussions. The swelling cells were kindly 3D-printed by CVT.AVT.

Author’s contribution

M.A. and T. P. performed swelling and stability experiments. R.G. and M.A. analyzed swelling kinetics and SDS stability curves and wrote the main manuscript.

Funding declaration

This research received no funding.

Conflict of Interest Statement

The authors of this work declare no conflict of interest.

Data Availability Statement

The datasets generated during the current study are available from the corresponding author on reasonable request.

References

1. Bouchoux, A., Gésan-Guiziou, G., Pérez, J., Cabane, B. (2010). How to squeeze a sponge: casein micelles under osmotic stress, a SAXS study. Biophys. J., 99, 3754–3762. https://doi.org/10.1016/j.bpj.2010.10.019
2. Broyard, C.; Gaucheron, F. (2015). Modifications of structures and functions of caseins: a scientific and technological challenge. Dairy Sci. & Technol., 95, 831–862. https://doi.org/10.1007/s13594-015-0220-y
3. Chang, C., Wang, T., Hu, Q., Zhou, M., Xue, J., & Luo, Y. (2017). Pectin coating improves physicochemical properties of caseinate/zein nanoparticles as oral delivery vehicles for curcumin. Food Hydrocolloids, 70, 143–151. https://doi.org/10.1016/j.foodhyd.2017.03.033
4. Dalgleish, D.G. (2010). On the structural models of bovine casein micelles—review and possible improvements. Soft Matter, 7, 2265–2272. https://doi.org/10.1039/C0SM00806K
5. Dalgleish, D. G., Corredig, M. (2012). The Structure of the Casein Micelle of Milk and Its Changes During Processing. Annu. Rev. Food Sci. Technol., 3:449–67. https://doi.org/10.1146/annurev-food-022811-101214
6. DeFrates, K., Markiewicz, T., Gallo, P., Rack, A., Weyhmiller, A., Jarmusik, B. & Hu, X. (2018). Protein polymer-based nanoparticles: Fabrication and medical applications. International journal of molecular sciences, 19(6), 1717. https://doi.org/10.3390/ijms19061717
7. de Kort, E., Minor, M., Snoeren, T., van Hooijdonk, T., & van der Linden, E. (2011). Effect of calcium chelators on physical changes in casein micelles in concentrated micellar casein solutions. International Dairy Journal, 21(12), 907–913. https://doi.org/10.1016/j.idairyj.2011.06.007.
8. de Kruif, C. G., Zhulina, E. B. (1996). k-Casein as a polyelectrolyte brush on the surface of casein micelles. Colloids and Surfaces A, 117, 151–159. https://doi.org/10.1016/0927-7757(96)03696-5
9. De Kruif, C.G., Huppertz, T., Urban, V.S. & Petukhov, A.V. (2012). Casein micelles and their internal structure. Advances in colloid and interface science, 171, 36–52. https://doi.org/10.1016/j.cis.2012.01.002
10. de Kruif, C. G., & Tuinier, R. (2001). Polysaccharide protein interactions. Food Hydrocolloids, 15(4–6), 555–563. https://doi.org/10.1016/S0268-005X(01)00076-5

11. Dumpler, J., Kieferle, I., Wohlschläger, H., & Kulozik, U. (2017). Milk ultrafiltrate analysis by ion chromatography and calcium activity for SMUF preparation for different scientific purposes and prediction of its supersaturation. International Dairy Journal, 68, 60–69. https://doi.org/10.1016/j.idairyj.2016.12.009
12. Gebhardt, R., Takeda, N., Kulozik, U., & Doster, W. (2011). Structure and stabilizing in- teractions of casein micelles probed by high-pressure light scattering and FTIR. The journal of physical chemistry. B., 115 (10), 2349–2359. https://doi.org/10.1021/jp107622d
13. Horne, D. S. (2002). Casein structure, self-assembly and gelation. Current Opinion in Colloid and Interface Science. 7, 5–6, 456–461. https://doi.org/10.1016/S1359-0294(02)00082-1.
14. Huppertz, T., Smiddy, M. A., de Kruif, C. G. (2007). Biocompatible protein micro-gel particles from cross-linked casein micelles. Biomacromolecules, 8, 1300–1305. https://doi.org/10.1021/bm061070m
15. Huppertz, T., de Kruif, C. G. (2008). Structure and stability of nanogel particles prepared by internal cross-linking of casein micelles. International Dairy Journal, 18, 556–565. https://doi.org/10.1016/j.idairyj.2007.10.009
16. Huppertz, T., Gazi I., Luyten, H., Nieuwenhuijse, H., Alting, A., Schokker, E. (2017). Hydration of casein micelles and caseinates: Implications for casein micelle structure. International Dairy Journal, 74, 1–11. https://doi.org/10.1016/j.idairyj.2017.03.006
17. Lefebvre-Cases, E., Gastaldi, E., de la Fuente, B. T. (1998). Influence of chemical agents on interactions in dairy products: Effect of SDS on casein micelles. Colloids and Surfaces B: Biointerfaces, 11, 281–285. https://doi.org/10.1016/S0927-7765(98)00054-X.
18. Liu, Y., Guo, R. (2007). Interaction between casein and sodium dodecyl sulfate. Journal of Colloid and Interface Science, 315, 685–692. https://doi.org/10.1016/j.jcis.2007.07.018
19. Liu, Y., Guo, R. (2008). Ph-dependent structures and properties of casein micelles. Biophysical Chemistry, 136(2–3), 67–73. https://doi.org/10.1016/j.bpc.2008.03.012.
20. Livney, Y.D. (2010). Milk proteins as vehicles for bioactives. Current Opinion in Colloid & Interface Science, 15, 73–83. https://doi.org/10.1016/j.cocis.2009.11.002
21. Marreto, R. N., Ramos, M. F., Silva, E. J., de Freitas, O., & de Freitas, L. A. (2013). Impact of cross-linking and drying method on drug delivery performance of casein–pectin microparticles. AAPS PharmSciTech, 14(3), pp.1227–1235. https://doi.org/10.1208/s12249-013-0012-8
22. McMahon, D. J., Oommen, B. S. (2008). Supramolecular Structure of the Casein Micelle. J. Dairy Sci., 91, 1709–1721. https://doi.org/10.3168/jds.2007-0819.
23. Sadiq, U., Gill, H., Chandrapala, J. (2021). Casein Micelles as an emerging Delivery System for Bioactive Food Components. *Foods*, 10(8), 1965. https://doi.org/10.3390/foods10081965
24. Schulte, J., Stöckermann, M., & Gebhardt, R. (2020a). Influence of pH on the stability and structure of single casein microparticles. Food Hydrocolloids, 105, 105741. https://doi.org/10.1016/j.foodhyd.2020.105741

25. Schulte, J., Stöckermann, M., Thill, S., & Gebhardt, R. (2020b). Calcium effect on the swelling behaviour and stability of casein microparticles. International Dairy Journal, 105, 104692. https://doi.org/10.1016/j.idairyj.2020.104692
26. Schulte, J., Pütz, T., Gebhardt, R. (2021). Statistical analysis of the swelling process of casein microparticles based on single particle measurements. Food Hydrocolloids for Health, 1, 100014. https://doi.org/10.1016/j.fhfh.2021.100014
27. Schulte, J., Pütz, T., Gebhardt, R. (2022). Influence of pectin and drying conditions on the structure, stability and swelling behavior of casein microparticles. *submitted*
28. Hens, B., & Bolger, M. B. (2019). Application of a dynamic fluid and pH model to simulate intraluminal and systemic concentrations of a weak base in GastroPlus™. Journal of Pharmaceutical Sciences, 108(1), 305–315. https://doi.org/10.1016/j.xphs.2018.10.041
29. Tuinier, R., & De Kruif, C. G. (2002). Stability of casein micelles in milk. The Journal of chemical physics, 117(3), 1290–1295. https://doi.org/10.1063/1.1484379
30. Yang, M., Wei, Y., Ashokkumar, M., Qin, J., Han, N., & Wang, Y. (2020). Effect of ultrasound on binding interaction between emodin and micellar casein and its microencapsulation at various temperatures. Ultrasonics sonochemistry, 62, 104861. https://doi.org/10.1016/j.ultsonch.2019.104861
31. Zahariev, N., Marudova, M., Milenkova, S., Uzunova, Y., & Pilicheva, B. (2021). Casein Micelles as Nanocarriers for Benzydamine Delivery. Polymers, 13(23), 4357. https://doi.org/10.3390/polym13244357
32. Zhuang, Y., Sterr, J., Kulozik, U., & Gebhardt, R. (2015). Application of con- focal Raman microscopy to investigate casein micro-particles in blend ca- sein/pectin films. International journal of biological macromolecules, 74, 44–48. https://doi.org/10.1016/j.ijbiomac.2014.11.017
33. Zhuang, Y., Sterr, J., Schulte, A., Kulozik, U. & Gebhardt, R. (2016). Casein microparticles from blend films forming casein/α-tocopherol emulsion droplets in solution. Food biophysics, 11(4), 332–338. https://doi.org/10.1007/s11483-016-9446-3

Figures

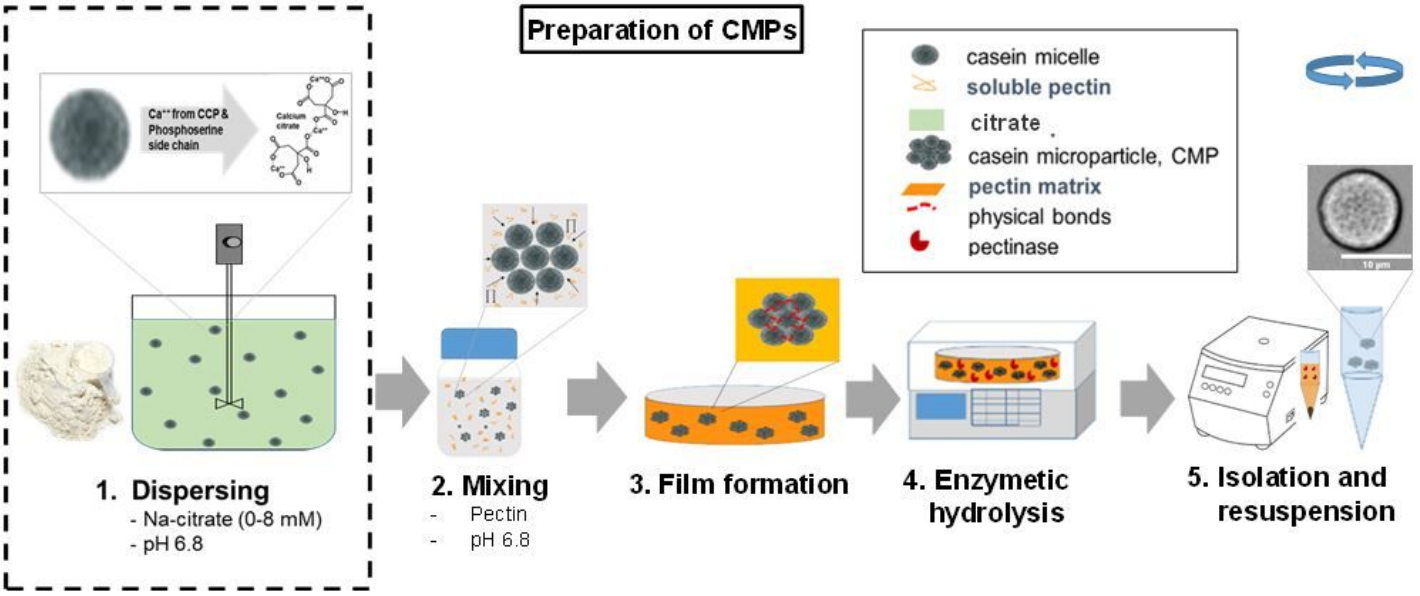

Figure 1

Process steps of producing casein microparticles

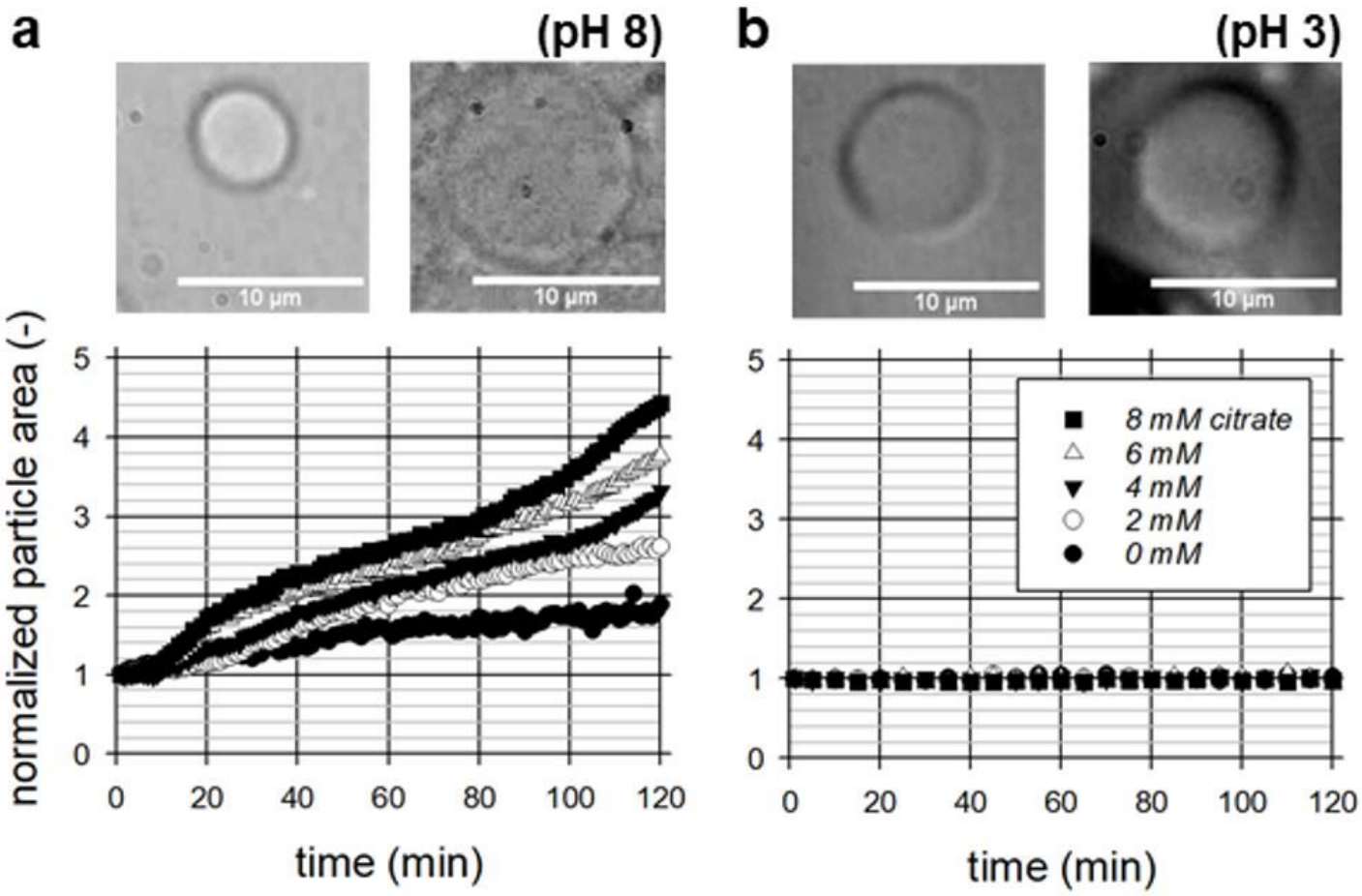

Figure 2

Microscopic images of CMPs with 8 mM citrate at the beginning and 120 min after pH change to pH8 (A) and pH 3 (B) occurred, and normalized swelling curves at different citrate concentrations each obtained by averaging two individual kinetics of the particle areas.

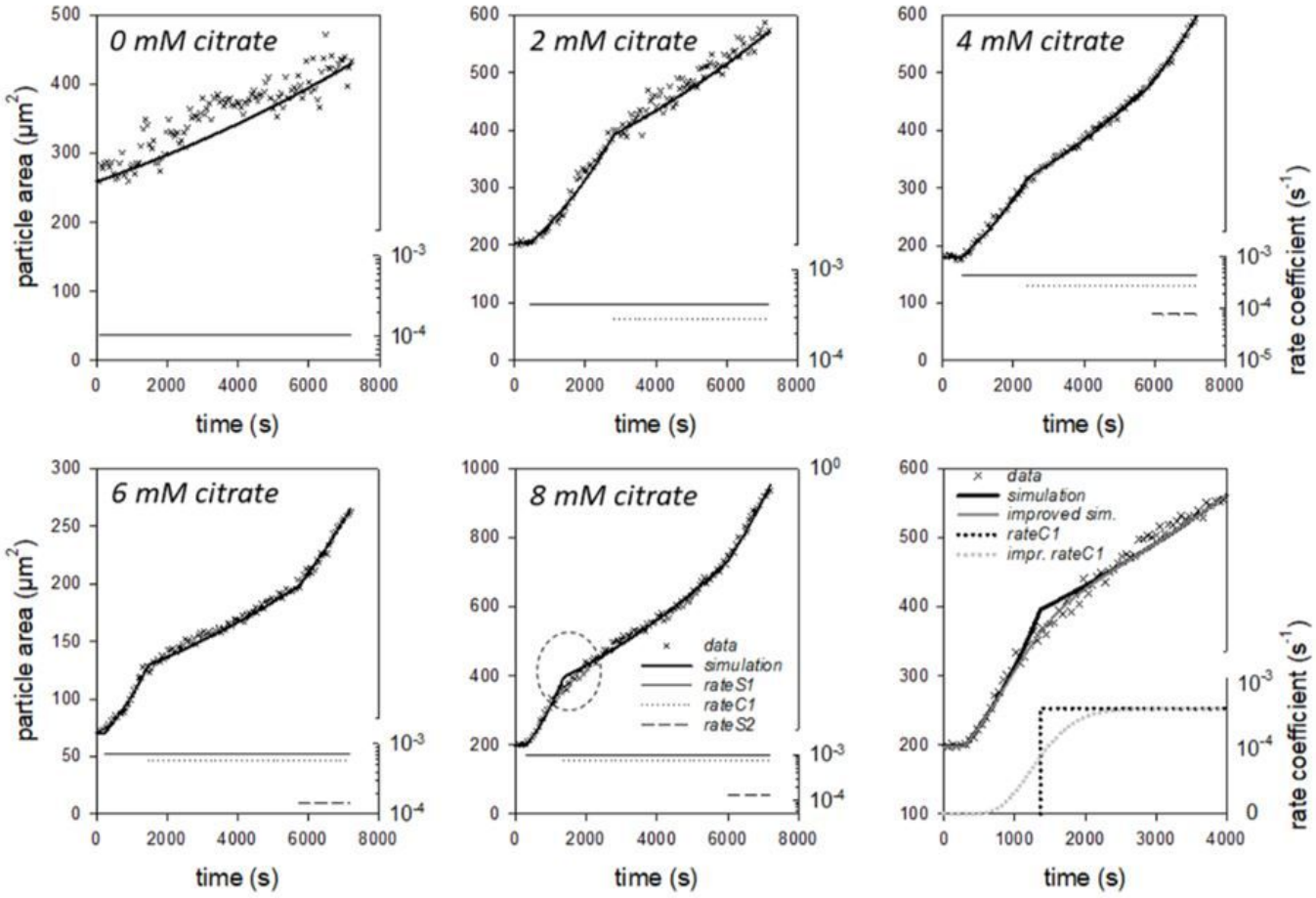

Figure 3

Individual swelling kinetics at pH 8 for CMPs, which were prepared without and with 2, 4, 6 and 8 mM citrate. The data correspond to the absolute particle areas and the lines are simulations with the dynamic swelling model. The values of the rate coefficients used from certain characteristic times via a step function to set the volume flows are also shown

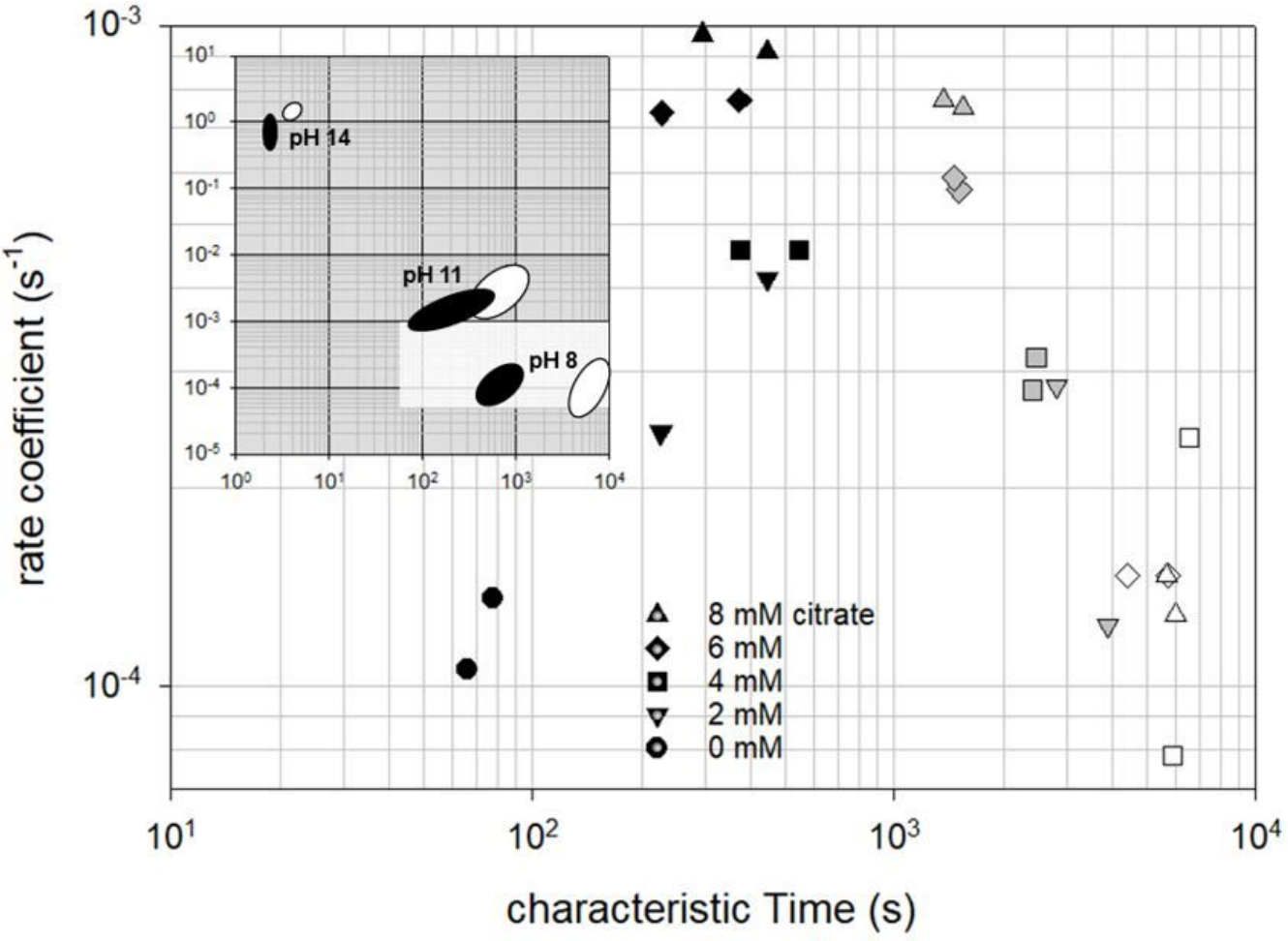

Figure 4

Swelling coefficients as a function of their characteristic start times for the first step (closed symbols) for the subsequent slowed phase (grey symbols) and for the second step (open symbols) of swelling of CMPs at pH 8.0 prepared without or with different citrate concentrations. The insert shows how the location of the parameter pairs for the first and second swelling steps of CMPs without citrates (black and white areas) changes as a function of pH (reconstructed from Schulte et al., 2020b)

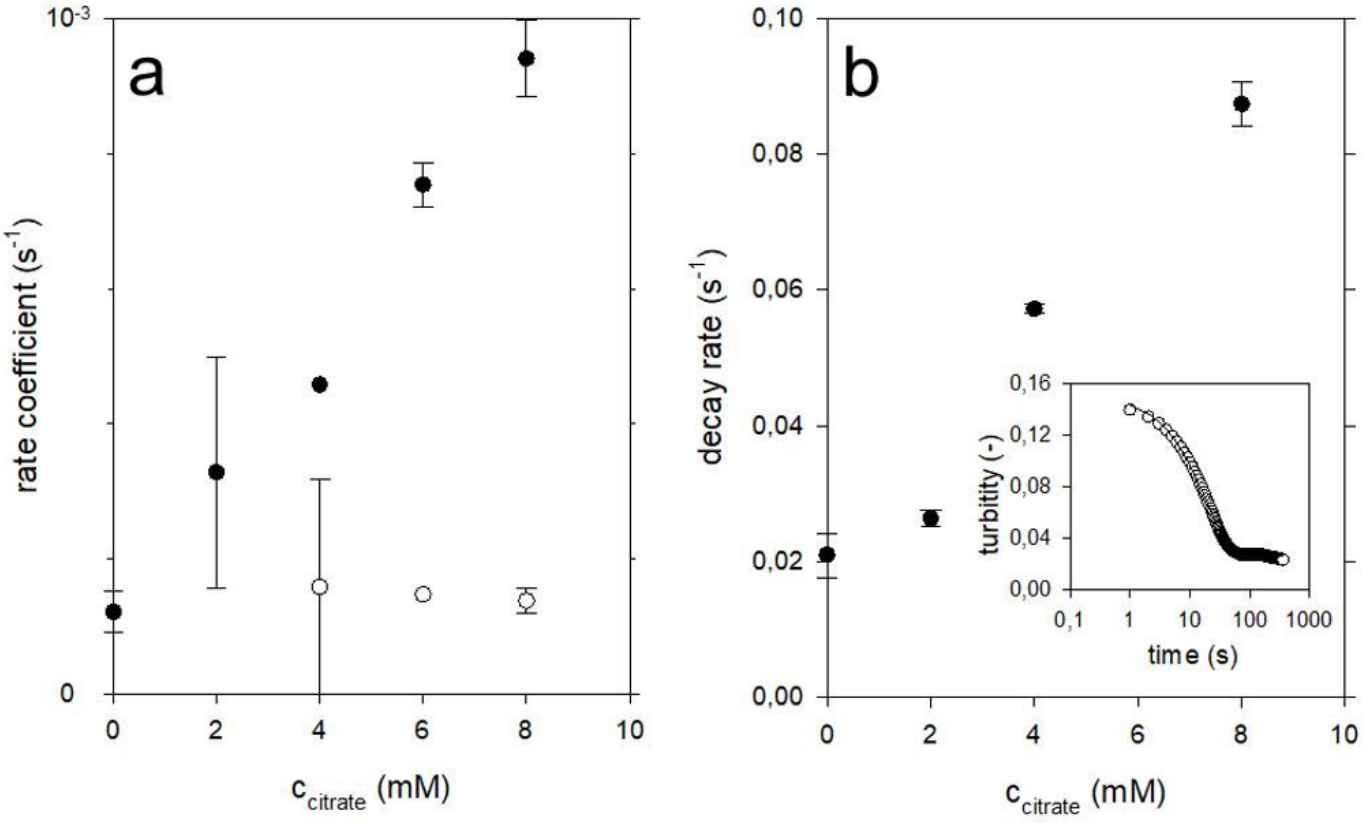

Figure 5

Rates determined from the swelling curves (a) and SDS-turbidity experiments (b) of CMP at pH 8 as a function of the citrate concentration used to prepare the particles